3.6. NON-LINEAR WASTE ROCK MODELLING

Matthew Otwinowski
University of Calgary

NON-LINEAR WASTE ROCK MODELLING

Matthew Otwinowski
Synergetic Technology, 139-31 Avenue N.W., Calgary AB, Canada T2M 2P1 and
The University of Calgary, Department of Physics and Astronomy, Calgary AB, Canada T2N 1N4; e-mail: motwinow@asc.ucalgary.ca

OUTLINE

APPENDIX

I. INTRODUCTION

This brief presentation reviews some recent results obtained during the development of a waste rock model.

By the research project agreement our recent modelling effort was limited to the analysis of acid rock drainage at pH values above 4.5 in the absence of bacterial oxidation [1].

The geochemical and thermodynamic behaviour of waste rock piles is significantly different from that of tailings. Unlike tailings, waste rock piles are not saturated with water. For this reason oxygen diffusion in waste rock piles is much faster than in tailings. At the same time, the thermal conductivity of waste rock piles is much smaller than the thermal conductivity of tailings. This causes a relatively slow transport of the heat generated by sulphide oxidation. Fast oxygen transport and slow heat removal are often responsible for fast acid generation rates due to the fast oxidation of sulphide minerals when high temperatures (often exceeding 40°C) develop inside waste rock piles. Rock reactivity, water flow, oxygen transport, and heat dissipation to the surroundings, are the main physical factors which control acid rock drainage for given mineral composition of waste rock. Both mass and energy transport depend on pile size, pile geometry and the ambient conditions.

Our previous scaling analysis[2], and the numerical results presented here show that large-scale thermodynamic effects (on a length scale greater than one metre) depend in a strongly nonlinear way, on the geochemical and physical properties at both the micro-scale (length scale less than 0.1) and meso-scale (1 cm to 1 m). The prediction of discharge values requires the understanding and proper description of the interplay between the geochemical and physical processes at all scales. The proper characterization of waste rock at all scales is very important for scaling-up laboratory data, and to enable one to address site-specific situations.

---

[1] A detailed analysis of the available experimental data on bacterial oxidation and chemical kinetics at pH below 4.5, is presented in our report "*Quantitative Analysis of Chemical and Biological Kinetics for the Acid Mine Drainage Problem*", MEND 1994.

[2] M. Otwinowski, "*Scaling Analysis of Acid Rock Drainage*", MEND 1995.

The geochemical, biological and physical processes responsible for acid rock drainage are strongly nonlinear.

- Sulphide oxidation rates accelerate with increasing temperature. The experimental data show a strongly nonlinear acceleration of the reaction rates in the temperature range observed in waste rock piles.

- Waste rock reactivity depends in a strongly nonlinear manner on particle size. We have performed a detailed geostatistical analysis of particle size distribution and its effect on rock reactivity and acid generation rates. In a typical ensemble of rock particles there are two important physico-chemical effects responsible for the increasing rock reactivity when particle size decreases:

  - Small particles have a large surface area per unit rock mass and the amount of sulphide exposed to oxygen dissolved in water film on rock surface increases with decreasing particle size.
  - The distance which oxygen has to travel through the micropores and cracks to reach reactive sulphide sites inside the rock particles, is short for small particles.

  The particle size distribution is characterized by a *fractal* distribution function.

- Field data show that the total discharge of contaminants is a strongly nonlinear function of the water flux.

- Waste rock piles may exhibit thermodynamic catastrophes associated with thermodynamic instabilities[3]. Such strongly nonlinear behaviour poses a serious difficulty for ARD prediction.

The strongly nonlinear features of acid rock drainage impose high requirements on the numerical and analytical methods used in a realistic model. We have used the finite element method with an adaptive grid generator.

---

[3]A thermodynamic catastrophe occurs when a small change of parameters such as pile size, ambient temperature, geochemical properties of waste rock, etc. causes a large change in overall acid generation rates.

II. THERMOKINETICS OF SULPHIDE OXIDATION

STOICHIOMETRIC EQUATIONS FOR PYRITE OXIDATION

$$FeS_2(s)+7/2\ O_2+H_2O = Fe^{2+}+2SO_4^{2-}+2H^+\ , \qquad (R1)$$

$$Fe^{2+}+1/4\ O_2+H^+ = Fe^{3+}+1/2\ H_2O\ , \qquad (R2)$$

$$FeS_2(s)+14Fe^{3+}+8H_2O = 15Fe^{2+}+2SO_4^{2-}+16H^+\ , \qquad (R3)$$

$$Fe^{3+}+3H_2O = Fe(OH)_3(s)+3H^+. \qquad (R4)$$

(R1) The oxidation of pyrite by molecular oxygen to Fe^{2+} and sulphate. The oxidation of iron sulphide (pyrite) to sulphate (eq. (R1)) releases dissolved ferrous ions and acidity into the water.

(R2) Subsequently, the dissolved ferrous ions undergo oxidation to ferric ions (eq. (R2)). This is a slow reaction and viewed as the rate-limiting step determining the overall rate of pyrite oxidation.

(R3) Sulphide is oxidized again by ferric ion and acidity is released along with additional ferrous ions which may re-enter the reaction cycle via reaction (R2). This is regarded as a fast step at pH less than 4.5.

(R4) Ferric ions hydrolyse to form insoluble ferric hydroxide (eq. (R3)), releasing more acidity to the stream. This reaction takes place only at high pH values which can be attained when the mineral composition of waste rock is such that self-buffering processes take place or when neutralizing minerals are added. *Reaction (R4) eliminates reaction (R3) at high pH values.*

At low pH values, reactions (R2) and (R3) provide a feedback loop discussed by Singer and Stumm (1970)[1] and Stumm and Morgan (1986)[2]. (Ferrous iron produced in (R3) is utilized again in reaction (R2)).

---

[1] P.C. Singer and W. Stumm, *"Acid Mine Drainage: The Rate Determining Step"*, Science **167**, 1121 (1970)

[2] W. Stumm and J.J. Morgan, *"Aquatic Chemistry. An Introduction Emphasizing Chemical Equilibria in Natural Waters"*, Wiley, 1986.

KINETIC EQUATIONS FOR PYRITE OXIDATION
Oxidation at pH between 4 and 7

Kinetic equations for pyrite oxidation have a form[1]:

$$\frac{d[Fe^{2+}]}{dt} = \frac{S}{V}k_1(T)[O_2]^{1/2} - k_2(T,[H^+])[Fe^{2+}][O_2] \ , \qquad (2.1)$$

$$\frac{d[Fe(OH)_3]}{dt} = k_2(T,[H^+])[Fe^{2+}][O_2] \ , \qquad (2.2)$$

$$\frac{d[H_2O]}{dt} = -\frac{S}{V}k_1(T)[O_2]^{1/2} - \frac{5}{2}k_2(T,[H^+])[Fe^{2+}][O_2] \ , \qquad (2.3)$$

$$\frac{d[O_2]}{dt} = -\frac{7S}{2V}k_1(T)[O_2]^{1/2} - \frac{1}{4}k_2(T,[H^+])[Fe^{2+}][O_2] \ , \qquad (2.4)$$

$$\frac{d[SO_4^{2-}]}{dt} = \frac{2S}{V}k_1(T)[O_2]^{1/2} \ , \qquad (2.5)$$

$$\frac{d[H^+]}{dt} = \frac{2S}{V}k_1(T)[O_2]^{1/2} + 2k_2(T,[H^+])[Fe^{2+}][O_2] \ . \qquad (2.6)$$

Rate constants k_1 and k_2 depend strongly on temperature. This is the dominant nonlinearity at the micro-scale, which is responsible for the strongly nonlinear thermodynamic behaviour of waste rock piles at the macro-scale.
The order p of the pyrite oxidation reaction with respect to the concentration of oxygen dissolved in water, $[O_2]$, is equal to ½. For p=1/2, the reduction of the oxygen concentration has a smaller effect on the reduction rates then for p=1. (For p=1 the oxidation rates are reduced by 50% when the oxygen concentration is reduced by 50%; for p=1/2 the oxidation rates are reduced by 50% when the oxygen concentration is reduced by 75% - this is important for the design of covers).

---

[1] M. Otwinowski, *"Quantitative Analysis of Chemical and Biological Kinetics for the Acid Mine Drainage Problem"*, MEND 1994

Temperature and pH dependence of reaction rates

$$k_1(T) = a \exp(-\frac{E}{RT}); \quad a = 8.5 \cdot 10^{-15}\,(mol)^{1/2} m^{-1/2} s^{-1},\ E = 88\ kJ/mol,\ R = 8.31\ Jmol^{-1} K^{-1}$$

$$k_2(T) = k_{21}(T) + k_{22}(T)[H^+]^{-1} + k_{23}(T)[H^+]^{-2}$$

$$k_{21}(T_o) = 1.30 \cdot 10^{-5} M^{-1} s^{-1}\ ,\quad k_{22}(T_o) = 1.41 \cdot 10^{-8} s^{-1}\ ,\quad k_{21}(T_o) = 3.78 \cdot 10^{-14} M s^{-1}\ .$$

$$k_{2i}(T) = k_{2i}(T_o) e^{\frac{E_{2i}(T-T_o)}{RTT_o}}\ , \qquad i = 1,2,3;$$

E_{21}=74kJ/mol , E_{22}=85kJ/mol , E_{23}=96kJ/mol .

The rate constants have been measured [1,2,3] at temperature T_o=20°C. Rate constants k_1 and k_2 are determined by measuring the molar oxidation rate per unit surface area of pyrite crystals and the molar concentration of oxygen dissolved in water (see also Table I). Pyrrhotite oxidizes much faster than pyrite.
For the activation energy of 70-90 kJ/mol reaction rates accelerate faster than by a factor of two per 10°C increase in temperature.

---

[1] M. A. McKibben and H. L. Barnes, Geochim. Cosmochim. Acta **51**, 793 (1987).
[2] B. Wehrli, in Aquatic Chemical Kinetics, W. Stumm ed., Willey, 1990.
[3] R.V. Nicholson et al., Geochim. Cosmochim. Acta **52**, 1077 (1988) & 54, 395 (1990).

SATURATION CONCENTRATIONS OF OXYGEN DISSOLVED IN WATER

T °C	$[O_2]_{gas}$=21%		$[O_2]_{gas}$=10%		$[O_2]_{gas}$=5%		$[O_2]_{gas}$=1%	
	mg	μmol	mg	μmol	mg	μmol	mg	μmol
10	11.30	353.0	5.31	165.9	2.59	80.9	0.41	12.8
20	9.12	284.9	4.23	132.2	2.01	62.8	0.23	7.2
30	7.60	237.5	3.44	107.5	1.56	48.7	0.05	1.6
40	6.47	202.1	2.81	87.8	1.15	35.9	0.00	0.0
50	5.57	174.0	2.25	70.3	0.74	23.1	0.00	0.0
60	4.89	152.8	1.64	51.2	0.25	7.8	0.00	0.0

Table I. Saturation concentrations of dissolved oxygen in water, $[O_2]$, at atmospheric pressure (1013.25 hPa) for different oxygen concentrations in the gaseous phase $[O_2]_{gas}$. The solubilities of oxygen are defined in terms of the mass of oxygen dissolved in one litre of the water in equilibrium with an atmosphere saturated with water vapour at various temperatures. The data are calculated following Benson and Krause (1980)[1] and using hydrological tables published by Beer (1991)[2].

Oxidation rates are controlled by temperature and oxygen concentration. Saturation values of oxygen dissolved in water decrease with temperature. This effect partly counteracts the temperature increase of oxidation rate[s]. The dependence of $[O_2]$ on $[O_2]_{gas}$ and T was disregarded in previous models. We were able to derive an analytical formula which describes the values of $[O_2](T,[O_2]_{gas})$. This formula is used in the model. (We will use notation $X=[O_2]$, $Y=[O_2]_{gas}$)

[1] B.B. Benson and D. Krouse, Jr., Limnol. Oceanogr., **25**, 662 (1980). [2] T. Beer, Applied Environmetrics, Victoria, Australia (1991).

IV. FRAGMENTATION OF ROCK AND FRACTAL PARTICLE SIZE DISTRIBUTION

A basic concept useful for understanding the fractal nature of fragmented rock is illustrated in Fig. 4.1. A zero-order cubic cell with dimensions h is divided into eight cubic elements each with dimension h/2. Two diagonally opposite cubes are retained at each scale. We have N_1=2 of particles with R_1=h/2, N_2=12 particles with R_2=h/4; fractal dimention d_f=2.58. This value of the fractal dimension (d_f=2.58) is very close to the experimental values for fragmented rock[1], presented in Fig. 4.2.

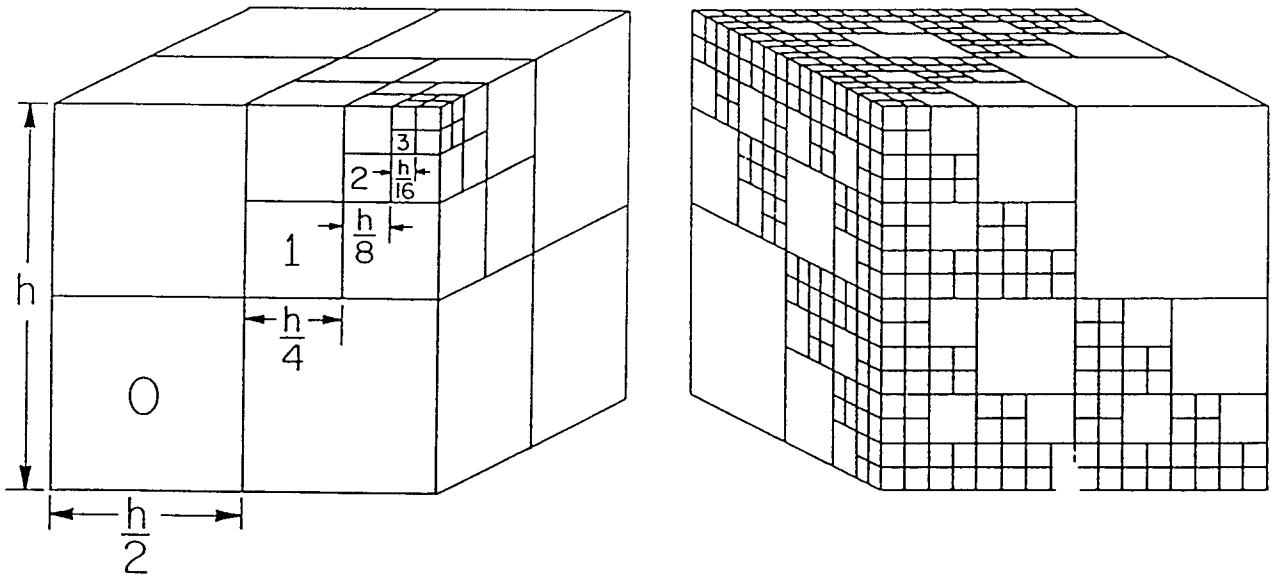

Fig. 4.1. An idealized model for fractal fragmentation: R_1=h/2, $N(>R_1)$=2; R_2 = h/4, $N(>R_2)$=14; R_3 = h/8, $N(>R_3)$=86; ...

The number N(>R) of fragments with a linear dimension greater than R is described by a relation

$$N(>R) = \frac{C}{R^{d_f}}$$

[1] If at a certain later stage the geometric division rule was changed, we would obtain a set of particles which cannot be described by a single fractal dimension value. Such a set is usually called a multifractal. The basic concepts of fractal geometry are presented in Appendix A.

The experimental data for the number N(R) of fragments with a size greater than R are presented in Fig. 4.2 for: broken coal[2], broken granite[3] from a 61 kt underground nuclear detonation, and impact ejecta due to 2.6 km/s projectile impacting on basalt[4].

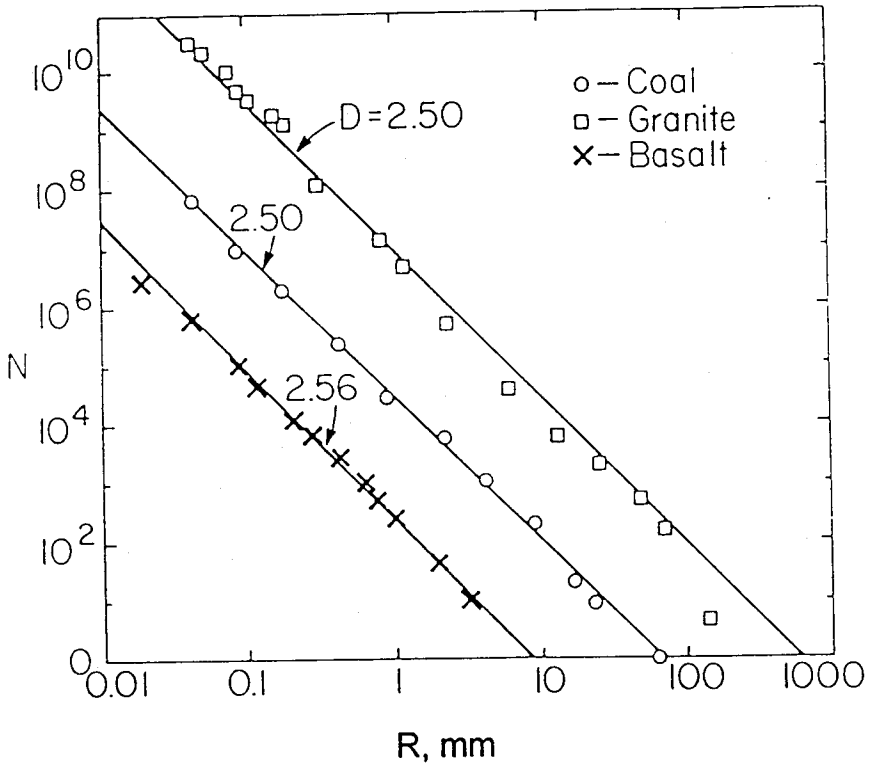

Fig. 4.2. Experimental data on the fragmentation of rock for different types of rock.

The distribution function N(R) is obtained from N(>R) as

$$N(R) \propto R^{-d_f - 1}$$

According to the fractal size distribution formula, in waste rock piles the number of particles grows dramatically with a decrease of particle size. We have used our results on the particle size dependence of leaching rates and the particle size distribution to derive geostatistical formulae for waste rock reactivity.

---

[2] J.G. Bennet , J. Inst. Fuel **10**, 22 (1936)..

[3] J.E. Schoutens, *"Empirical analysis of nuclear and high-explosive cratering and ejecta"*, in Nuclear Geoplosics Sourcebook, 55, Def. Nuclear Agency, 1979.

[4] A.G. Fujiwara A., G. Kamimoto and A. Tsukamoto, Icarus **31**, 277 (1977).

V. GEOSTATISTICAL FORMULAE FOR WASTE ROCK REACTIVITY

SCALING UP LABORATORY DATA: FROM MICRO-SCALE TO MESO-SCALE

One of the crucial problems in ARD prediction is how to use the laboratory data obtained during leaching tests to estimate oxidation rates and acid generation rates in the field. Leaching tests are usually designed to generate information about the chemical composition of the leachate, often disregarding the physical aspects of rock reactivity. We analysed the physical effect of the variable particle size on oxidation rates and the consumption of oxygen per unit mass of waste rock in waste rock piles. These results are a very significant component of a large scale waste rock model. We adopt the approach in which the chemical properties of the waste rock can be characterized as quantities averaged over a volume of about 1 m^3. (Rock particles greater than 1 m can be explicitly included in a large-scale model.) This type of physical and statistical characterization of waste rock leads to a relatively simple set of equations describing the oxygen consumption rates and transport of mass and energy in waste rock piles.

In order to calculate the oxidation rate for an ensemble of particles we have to combine information about the size-dependent oxidation rates for individual particles and the fractal distribution of particle size. Oxidation rates per particle scale with particle size R as R^{α} with $\alpha>0$. Our calculations show that $\alpha=2$ for surface dominated oxidation, and $\alpha=1$ for volume dominated oxidation[1].

SURFACE DOMINATED OXIDATION RATES

$$Rate_{surf}(R_{\min}, R_{\max}; M) = \frac{CV}{R_{\exp}^2 M}\int_{R_{\min}}^{R_{\max}} x^2 N(x)\,dx = \frac{nCV}{(1-n)MR_{\exp}^2 R_{\max}}\left[\left(\frac{R_{\max}}{R_{\min}}\right)^{1-n} - 1\right]$$

$$n=3-d_f$$

---

[1] At the initial stage of ARD, acid is generated mostly due to the oxidation of sulphide minerals on the particle surface. When a large portion of the sulphide on the rock surface is oxidized, the oxidation of the sulphide inside the rock particles becomes increasingly important. These two stages are called *surface dominated* and *volume dominated* oxidation.

VOLUME DOMINATED OXIDATION RATES

$$Rate_{vol}(R_{min}, R_{max}; M) = \frac{CV}{x_{exp} M} \int_{R_{min}}^{R_{max}} xN(x)\,dx = \frac{nCV}{(2-n)MR_{exp}R_{max}^2}\left[\left(\frac{R_{max}}{R_{min}}\right)^{2-n} - 1\right]$$

Mass M is given by:

$$M = \rho\, R_{max}\left[1 - (R_{min}/R_{max})\right]^{n+1} .$$

The geostatistical formulae[2] allow one to estimate the reactivity of a unit mass of waste rock with a particle size between R_{min} and R_{max}, based on results of leaching tests performed by using particles of size R_{exp}. (ρ is rock density; V is volume; C is a constant determined during leaching tests; C carries information about sulphide content, rock porosity and other geochemical and physical properties of waste rock). $Rate_{vol}$ and $Rate_{surf}$ can be expressed in terms of a chemical rate constant a and effective reactive surface area per unit volume, σ.

The geostatistical formulae are very important for translating results of laboratory leaching tests into field situations.

Some of the previous models used Gaussian or Poisson particle size distribution. Such models should not be used for the interpretation of the laboratory leaching tests because they significantly underestimate the number of small rock particles and give unrealistic estimates for waste rock reactivity.

The geostatistical formulae give the oxidation rates per unit mass at the values of temperature and oxygen partial pressure for which a value of reaction constant C is measured during laboratory tests. A large-scale model evaluates the total sulphide oxidation and acid generation rates inside a waste rock pile with spatially nonhomogeneous distribution of oxygen and temperature.

---

[2] It is worthy of note that analogous results are impossible to obtain without referring to numerical integration when the Gaussian or Poisson distributions are used instead of fractal distribution for particle size. Apart from giving the correct description of fragmented rock, fractal distribution has an additional advantage of greatly simplifying the computer code used for a waste rock model.

ROCK FRAGMENTATION BY EQUIPMENT TRAFFIC

Equipment traffic during the different stages of pile construction is responsible for the formation of layers with small particles. The oxidation rates in the small particle layers are much greater than in the rest of the pile.

As an illustration of the application of the geostatistical formulae for rock activity we calculate a change in rock reactivity when the maximum size R_{max} decreases from R_{max} = 50 cm to R_{max} = 10 cm, where d_f = 2.5 in both examples.

Volume dominated oxidation

R_{max} = 50 cm $Rate_{vol}$ (R_{min}=1 cm, R_{max}=50 cm)=9.34×10^{-4} C_{vol} V/M

↓ ↓

R_{max} = 10 cm $Rate_{vol}$ (R_{min}=1 cm, R_{max}=10 cm)=1.02×10^{-2} C_{vol} V/M

eleven times faster

Surface dominated oxidation

R_{max} = 50 cm $Rate_{surf}$ (R_{min}=1 cm, R_{max}=50 cm)=2.43×10^{-3} C_{surf} V/M

↓ ↓

R_{max} = 10 cm $Rate_{surf}$ (R_{min}=1 cm, R_{max}=10 cm)=1.32×10^{-2} C_{surf} V/M

five times faster

During the surface dominated oxidation the rates are faster than during the volume dominated oxidation ($C_{surf} > C_{vol}$). However, the particle size effect is stronger during the volume dominated stage than during the initial surface dominated stage.

During the volume dominated stage of oxidation, the release of contaminant is controlled, among other factors, by particle size and the rate of diffusion of reaction products from sulphide sites in the pores to the surface of porous rock (reaction products are temporarily stored in the rock particles and we call this phenomenon a storage tank effect).

VI. REACTION - DIFFUSION - CONVECTION MODEL

$$\epsilon \frac{\partial Y}{\partial t} = \epsilon D \nabla^2 Y + \epsilon \left(\frac{\partial \psi}{\partial z}\frac{\partial Y}{\partial x} - \frac{\partial \psi}{\partial x}\frac{\partial Y}{\partial z}\right) - (1-\epsilon) a \sigma [X(Y,T)]^p \exp[-E/(RT)]$$

I II III IV

$$[\epsilon \rho_a C_a + (1-\epsilon)\rho_r C_r]\frac{\partial T}{\partial t} = \lambda \nabla^2 T + \epsilon(\rho_a C_a + r\mu Q_w)\left(\frac{\partial \psi}{\partial z}\frac{\partial T}{\partial x} - \frac{\partial \psi}{\partial x}\frac{\partial T}{\partial z}\right) + h(1-\epsilon) a\sigma [X(Y,T)]^p \exp[-E/(RT)]$$

V VI VII VIII

$$\nabla^2 \psi = Ra \frac{\partial T}{\partial x}; \qquad \left(-\frac{\partial \psi}{\partial z}, \frac{\partial \psi}{\partial x}\right) = (v_x, v_z)$$

Ra is the thermal Rayleigh number for air. The velocity components v_x and v_z are defined by the derivatives of the stream field. The change of energy density associated with the convective vapour transport is expressed as

$$X(Y,T) = [O_2] \ , \quad Y = [O_2]_{gas}; \qquad \mu = 1.6 \cdot 10^{-3}\ kg\, m^{-3} K^{-1} \ ,$$

$X(Y,T)$ denotes the local concentration of oxygen dissolved in water which is given by a closed form formula as a function of temperature and oxygen concentration in the gas phase (see Table I), r is the relative humidity (greater than zero and less than one), v is flow velocity, Q_w - latent heat of evaporation; $Q_w = 2.45 \cdot 10^6$ J kg^{-1}. At velocity values on the order of 10^{-4} m/s the energy transport rate due to convective vapour transport becomes comparable to the rate of heat transfer by thermal conduction.

The individual terms represent [1] :

I the total (local) rate at which oxygen concentration changes in the gas phase inside the pile

II the diffusive transport of oxygen through the pile pores

III the convective transport of oxygen through the pile pores

IV the rate at which oxygen is depleted due to the oxidation reactions

V the total (local) rate at which the thermal energy density changes inside the pile

VI the thermal conductivity of waste rock + air

VII the convective cooling due to convective flow of air with water vapour

VIII the energy generation due to exothermic sulphide oxidation

---

[1] The finite element method with an adaptive grid generator for a fully coupled set of the nonlinear reaction-diffusion-convection equations has been used to analyse the nonlinear processes responsible for ARD. Iterative schemes which decouple the set of equations do not produce reliable results.

One of our objectives was to obtain numerical results which would indicate how sulphide oxidation rates per unit rock mass are affected by the pile height, volume and shape. Two different types of piles analysed in our simulations are depicted in Fig. 6.1. Pile A has a square base of length s1 and a square top of a length s2; s1=100 m, s2=90 m. Pile B has dimensions s1=100 m and s2=60 m. Pile C is much smaller and has the values of s1=40 m and s2=30 m. We have obtained numerical solutions for piles with different height L.

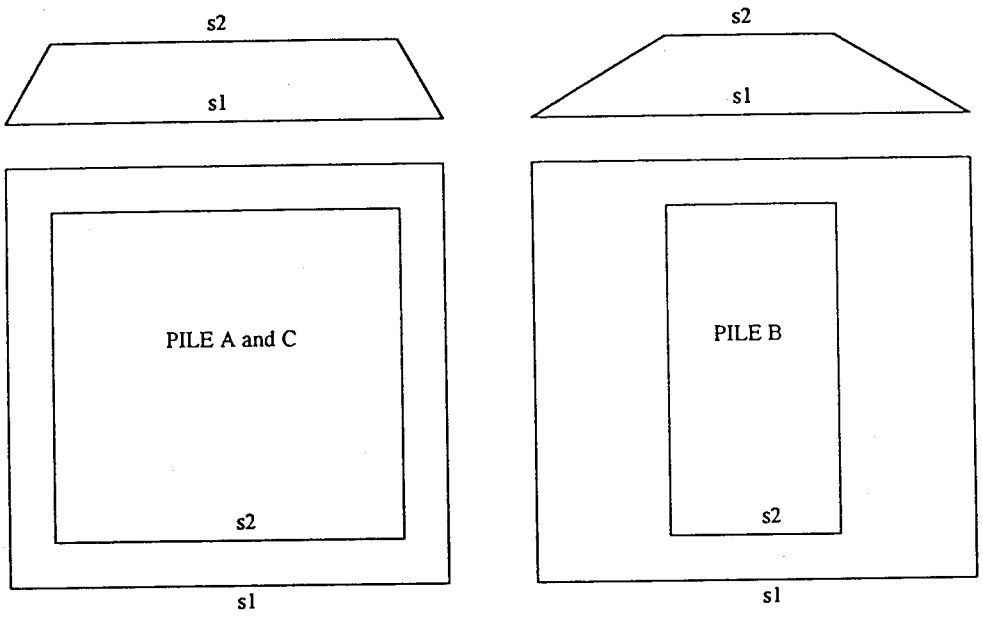

Fig. 6.1. Two types of piles with different slopes considered in numerical simulations.

Table II contains the input parameters used during the numerical simulation. The boundary conditions for oxygen concentration Y_{s1} assume that the bedrock porosity is five times smaller than the pile porosity.

TABLE II.

$\epsilon = 0.20$	(pile porosity)
$\lambda(\epsilon) = 0.18$ J/(s m °C)	(thermal conductivity)
$h = 0.41$ MJ/mol	(heat of pyrite oxidation per mol of oxygen consumed)
$D = 2.0 \cdot 10^{-5}$ m^2/s	(oxygen diffusion constant)
$a = 31.9 \cdot 10^{-15}$ mol$^{1/2}$m$^{-1/2}$s^{-1}	(kinetic coefficient of the oxidation reaction)
$\sigma = 0.5$ m^{-1}	(effective surface area of pyrite exposed to oxidation in 1m^3 of pile volume)
E=88 kJ/mol	(activation energy of the oxidation reaction)
p=1/2	(order of the reaction with respect to the oxygen conc.)
$T_{s1} = 12$°C	(temperature at the bottom)
$T_{s2} = 15$°C	(temperature at the pile surface)
$Y_{s1} = 1.88$ mol/m^3	(oxygen concentration at the pile-bedrock interface)
$Y_{s1} = 9.38$ mol/m^3	(oxygen concentration at the pile surface)

Table III summarizes the important information about :

- total acid generation rates measured as the total number of moles of sulphate generated inside the pile (denoted by SULtot)
- average acid generation rate per one cubic metre of waste rock per hour (SULav)
- spatial variability of acid generation rates measured as the minimum and the maximum local sulphate generation rates in moles of sulphate generated per one cubic metre of waste rock per hour (SULmin and SULmax)
- average concentration of oxygen (Yav)
- maximum temperature inside the pile (Tmax)
- total energy generation rate (Etot)
- maximum local energy generation rates per one cubic metre per hour (Emax)
- average energy generation rate (Eav)
- total thermal energy stored (Est) calculated as the volume integral

$$E_{st} = (\rho_r C_r + \rho_a C_a) \int_V T dV$$

(Only the difference between the stored energy for different piles has a physical meaning because the energy is determined up to an additive constant. An additive constant is different for piles of different size and only piles of the same type A, B or C can be compared).

Piles with different shapes and size but the same height L have the same values of maximum temperature.

The maximum temperature and the oxidation rates increase with the pile height L. For example, piles A6.0, B6.0 and C6.0 have exactly the same maximum temperature and the same maximum (local) sulphate generation rates.

Piles A6.0 and C6.0 have the same average sulphate generation rates per unit waste rock mass, despite a significant difference in the lateral dimensions (piles A have the base 100 m by 100 m, piles C have the base 40 m by 40 m and contain much less waste rock than piles A). Piles B do not have steep slopes and produce less acid per unit waste rock mass than the piles A and B of the same maximum height.

The rate of energy generation increases with pile height. Energy generation rates are proportional to the acid generation rates. Piles A, B, and C have different volumes and for this reason they generate different amounts of energy per unit time (Etot). The total stored energy Est also increases with the pile size.

Numerical results for piles of different size, shape and different sulphide content

Pile symbol	Total sulphate SULtot $mol(m^3h)^{-1}$	Average sulphate SULav $mol(m^3h)^{-1}$	Minimum sulphate SULmin $mol(m^3h)^{-1}$	Maximum sulphate SULmax $mol(m^3h)^{-1}$	Max. temp. Tmax °C	Average oxygen Yav mol/m^3	Total energy Etot 10^6Jh^{-1}	Max. energy Emax $J(m^3h)^{-1}$	Average energy Eav $J(m^3h)^{-1}$	Stored energy Est
A6.0	11.7	$2.05x10^{-4}$	$0.87x10^{-4}$	$3.0x10^{-4}$	15.3	5.62	2.39	62	44	8567
B6.0	8.66	$0.96x10^{-4}$	$0.87x10^{-4}$	$3.0x10^{-4}$	15.3	5.58	1.77	62	41	6340
C6.0	1.52	$2.08x10^{-4}$	$0.87x10^{-4}$	$3.0x10^{-4}$	15.3	4.23	0.89	62	42	2977
A8.0	15.9	$2.20x10^{-4}$	$0.87x10^{-4}$	$3.0x10^{-4}$	15.9	5.59	3.42	65	46	11239
SA11.3/8	11.3	$1.10x10^{-4}$	$0.87x10^{-4}$	$1.2x10^{-4}$	15.9	5.66	2.43	24	23	15899
B8.0	12.25	$1.36x10^{-4}$	$0.87x10^{-4}$	$3.0x10^{-4}$	15.9	5.54	2.63	65	44	8771
C8.0	2.17	$2.21x10^{-4}$	$0.87x10^{-4}$	$3.0x10^{-4}$	15.9	5.77	1.28	65	41	2977
A10.0	22.1	$2.45x10^{-4}$	$0.87x10^{-4}$	$3.3x10^{-4}$	17.4	5.52	4.53	68	50	14970
B10.0	16.8	$2.35x10^{-4}$	$0.87x10^{-4}$	$3.3x10^{-4}$	17.4	4.32	3.44	68	39	11551
C10.0	3.01	$2.45x10^{-4}$	$0.87x10^{-4}$	$3.3x10^{-4}$	17.4	5.79	1.77	68	39	5451
A12.0	32.7	$3.02x10^{-4}$	$0.87x10^{-4}$	$4.3x10^{-4}$	20.6	5.36	7.09	89	62	20061
SA17/12	23.2	$1.51x10^{-4}$	$0.87x10^{-4}$	$2.1x10^{-4}$	20.6	5.47	5.03	45	30	28292
A15.0	65.2	$4.82x10^{-4}$	$0.87x10^{-4}$	$9.5x10^{-4}$	29.0	5.20	10.3	206	85	28548
A15.1	71.1	$5.22x10^{-4}$	$0.87x10^{-4}$	$14.2x10^{-4}$	32.9	5.11	15.3	293	107	31211

TABLE III. The symbols in the first column refer to the pile lateral dimensions and height in metres. Piles A, B and C have different shapes and are defined in Fig. 6.1. The value of the reactive surface area σ per unit volume is equal to 0.5 m^{-1} for piles A, B, and C. Piles SA11.3/8 and SA17/12 have $\sigma=0.25$ m^{-1} and height greater by a factor of $2^{1/2}$ than the height of piles A8.0 and A12.0 respectively. The ratio between the total mass of waste rock in piles A, B and C of the same height is about 7/5/1. (See text for further explanation and discussion).

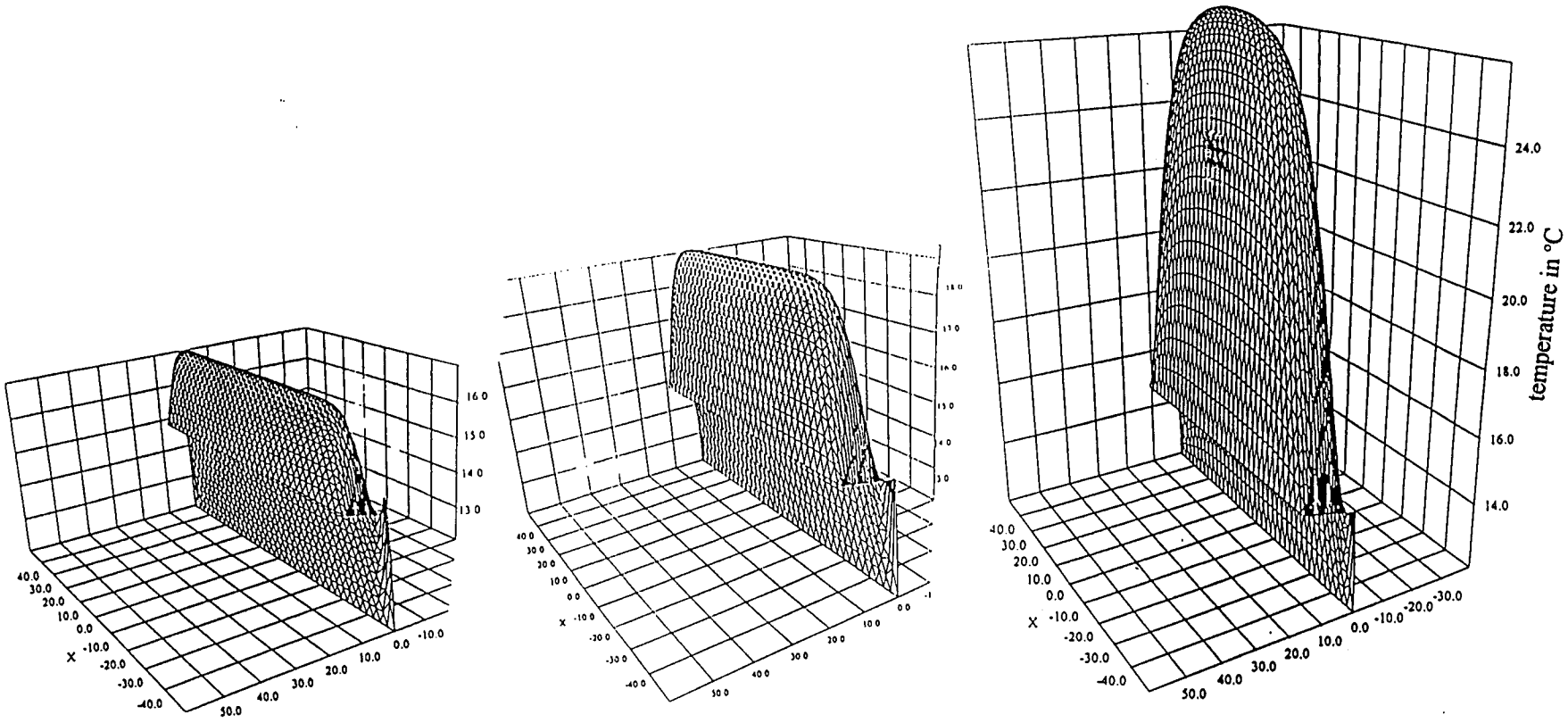

Fig. 6.1. Temperature distribution in piles (from left to right) A10.0, A11.5 and A13.0 (here and in other figures pile height shown along Y-axis). The three-dimensional plots show a strongly nonlinear increase of temperature when the pile height increases.

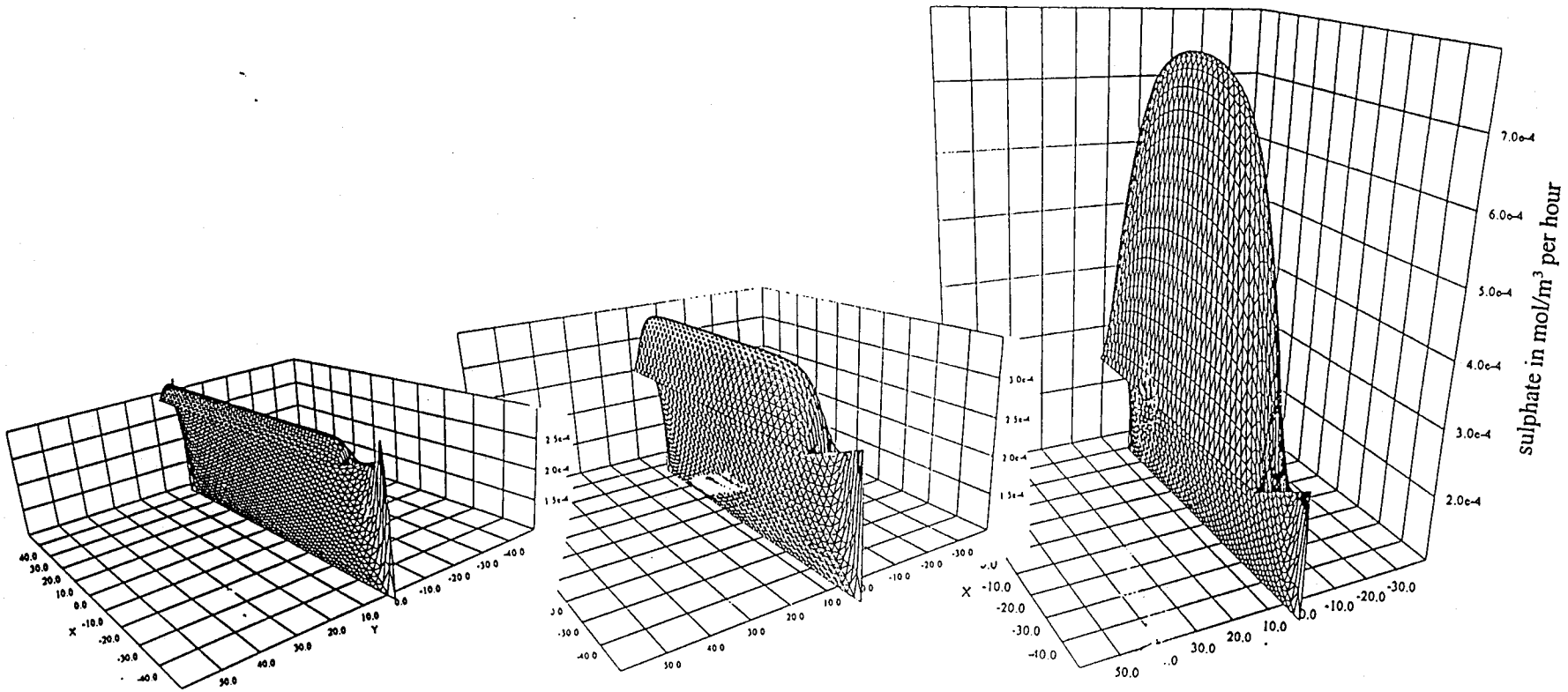

Fig. 6.2. Sulphate generation rates in piles (from left to right) A10.0, A11.5, and A13.0. Note that the maximum oxidation rates coincide with the temperature maxima in Fig. 6.1.

SCALING PROPERTIES

Piles SA11.3/8 and SA17/12 have the values of L greater by a factor of $2^{1/2}$ and contain a less reactive waste rock, with σ=0.25, smaller by a factor of two than σ=0.5 in their counterparts, piles A8.0 and A12.0.

Piles A8.0 and SA11.3/8 have exactly the same maximum temperature, and average thermal energies different by a factor of two. Piles A12.0 and SA17/12 also have exactly the same maximum temperature, and average thermal energies different by a factor of two. The average acid generation rate in pile SA17/12 are also slower by a factor of two than in pile A12.0. The ratios between the height and rock reactivity of piles SA17/12 and A12 are again $2^{1/2}$ and ½, respectively. In pile SA17/12 the total acid generation rate is by a factor of $2^{1/2}$ *smaller* than in pile A12.

The numerical results confirm our earlier results of the scaling analysis[1]. The large-scale properties of waste rock piles are governed by a scaling parameter[2]

$$\delta \propto L\sqrt{\frac{\sigma(1-\epsilon)}{D\epsilon}}$$

Because the oxidation rate and energy generation rate are proportional to σ it is obvious that after a transformation $L \to 2^{1/2}L$ and $\sigma \to \sigma/2$ we should obtain a pile with the same maximum temperature but the average oxidation rate per unit mass reduced by a factor of $2^{1/2}$.

Piles with the same values of δ are expected to have the same properties.

The numerical and analytical (scaling) results show that the physical features of the pile design are as important as the geochemical properties of the waste rock.

---

[1] M. Otwinowski, *"Scaling Analysis of Acid Rock Drainage"*, MEND Report (1994).

[2] A complete scaling formula which includes the remaining model parameters will be presented in our forthcoming publications.

VII. THERMODYNAMIC CATASTROPHES AND THEIR EFFECT ON ACID GENERATION RATES IN WASTE ROCK PILES

The numerical results show that at certain critical parameter values, the thermodynamic system may exhibit a sharp transition to a high energy state characterized by dramatically faster oxidation rates. We call this transition a *thermodynamic catastrophe.* Thermodynamic catastrophes are associated with the bifurcation properties of the nonlinear reaction-transport problems.

The total sulphate generation rates, the average sulphate generation rates and the maximum sulphate generation rates increase significantly with pile height. In Table III, piles which are 6 m and 8 m high have very similar sulphate acid generation rates. This happens because at low temperatures the decrease in oxygen concentration in larger piles is sufficient to counteract the effect a small increase of temperature has on the oxidation rates.

By increasing the height of above ten metres one observes a strongly nonlinear increase in temperature, accompanied by a very dramatic increase in the acid generation rates. At a height of L^*=14.5 metres a thermodynamic catastrophe takes place[1]. The average acid generation rates in piles A15.0 and A15.1 are more than 300% faster than in pile A12.0 which is only 25% smaller. By increasing the pile height from 12 m to 15 m, the maximum temperature increases by about 10°C. This is sufficient to increase the oxidation rates very dramatically. Piles A15.0 and 15.1 are in a critical thermodynamic state and generate much more acid than the lower piles. The maximum acid generation rate in pile A15.1 is about 50% greater than in pile A15.0 which is only 0.1 m lower. This is a direct result of a thermodynamic instability. In large piles, the energy dissipation rates are insufficient to counteract the energy generation rates. The maximum energy generation rate in pile A15.5 is about 5 times greater than in the smaller piles. Energy is generated very rapidly in warm spots which are formed when the thermodynamic dissipative structure of temperature and oxygen concentration becomes unstable. This process is illustrated by the three-dimensional plots in Figs. 7.1-7.2.

---

[1] We chose the pile height as a critical parameter as an example only. Other *combined* geochemical and physical effects also lead to the critical thermodynamic behaviour.

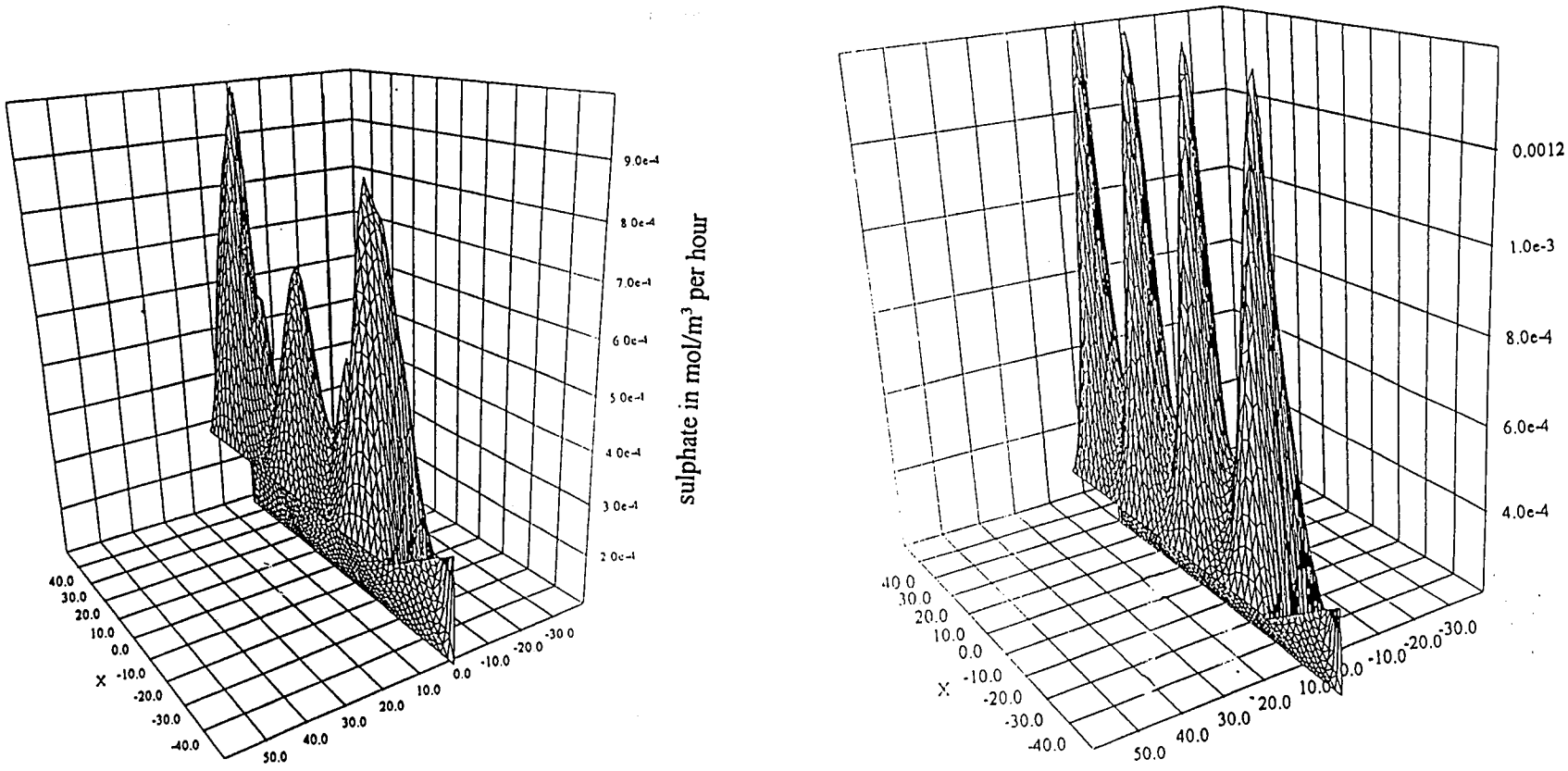

Fig. 7.1. Sulphate generation rates in piles A15.0 (left) and A15.1 (right). Note that in the critical region associated with thermodynamic catastrophes, large horizontal gradients of acid generation rates develop. (The regular pattern results from the regular trapezoidal pile shape - irregular piles show irregular spatial distribution of temperature, oxygen and acid generation rates).

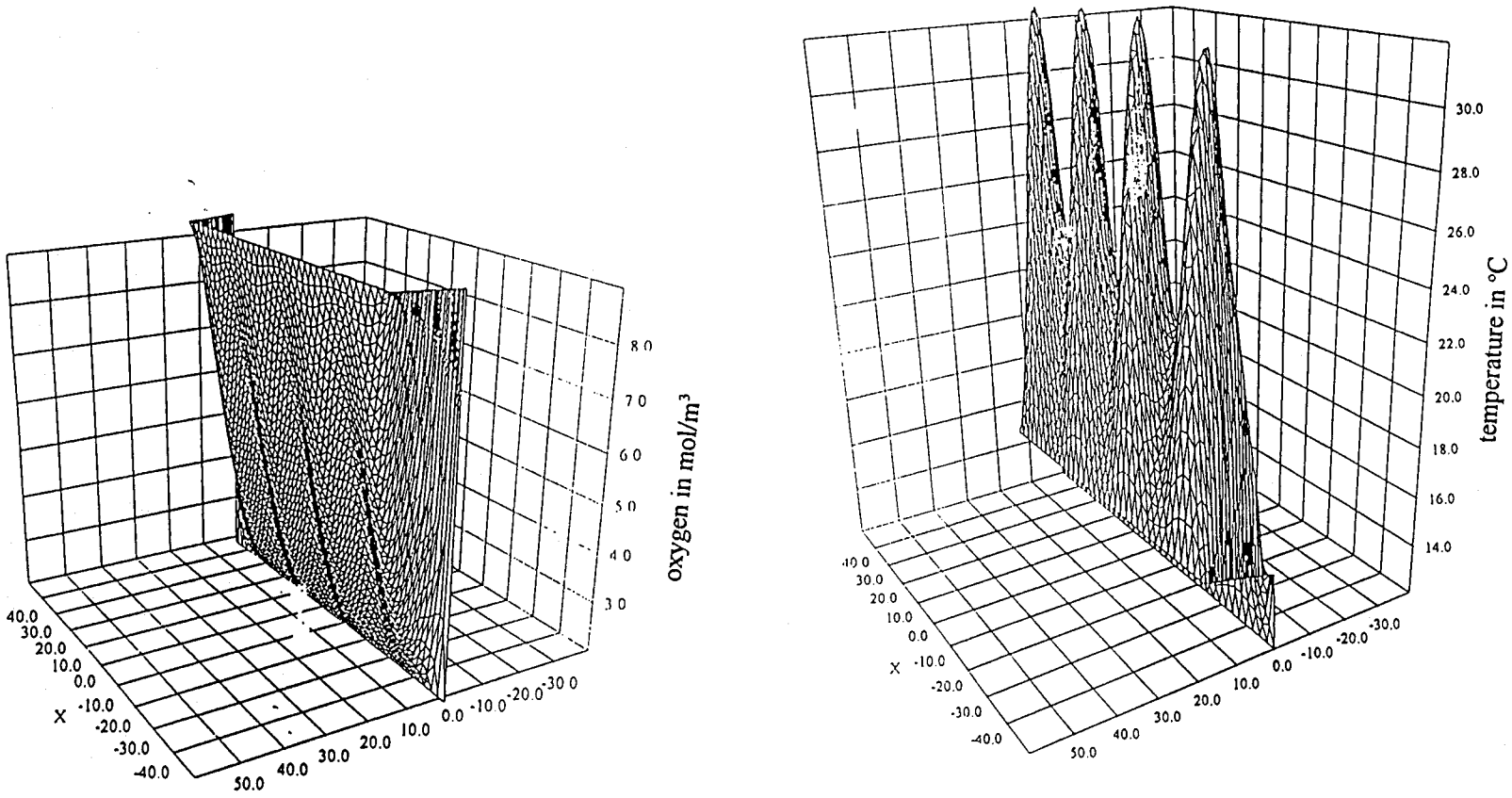

Fig. 7.2. Temperature and oxygen concentration profiles in pile A15.1. (Large horizontal temperature gradients trigger fast convective flow in the whole volume of the pile).

VIII. EFFECTIVENESS OF IMPERMEABLE COVERS

In Table IV, the results for four different piles with covers and impermeable lining of different thickness are presented. The diffusion coefficient inside the covers is assumed to be 1.0×10^{-8} m^2/s. In each case the cover and lining thickness is selected so that the same values of oxygen concentration, $Y_{s1}=Y_{s2}=1.17$ mol/m^3, at the cover - waste rock interface and at the lining - waste rock interface are produced. Covers are responsible for a significant reduction of oxygen concentration to a value of 1/8 of the normal atmospheric value. From examples summarized in Table IV it is evident that in order to generate the same reduction in oxygen concentration, when the pile height increases linearly (subsequent values of L are equal to 10, 15, 20 and 30 metres), the cover thickness has to increase in a nonlinear way (subsequent values of cover thickness d are 0.45, 0.85, 1.20 and 1.50 metre, respectively).

A very important feature of our results is the indication that *the critical size effect and thermodynamic catastrophes can be eliminated by covers of sufficiently low permeability.*

In Fig. 8.1, pile A30.0C has a completely different spatial distribution of oxidation rates than in the lower piles. When covers of sufficiently low permeability are used, one can create a situation in which the average acid generation rate can be decreased by increasing the pile height. By limiting the transport of oxygen through the boundaries one can create the situation in which the pile height can be increased infinitely. A cover breakdown will have, however, dramatic consequences in high piles. The risk factor increases with the pile height.

Numerical results for piles of different size, different cover permeability and different fine particle content

Pile symbol and cover thickness d	Total sulphate SULtot $mol(m^3h)^{-1}$	Average sulphate SULav $mol(m^3h)^{-1}$	Minimum sulphate SULmin $mol(m^3h)^{-1}$	Maximum sulphate SULmax $mol(m^3h)^{-1}$	Max. temp. Tmax °C	Average oxygen Yav mol/m^3	Total energy Etot 10^6Jh^{-1}	Max. energy Emax $J(m^3h)^{-1}$	Average energy Eav $J(m^3h)^{-1}$
A10.0 no cover	22.1	$2.45x10^{-4}$	$0.87x10^{-4}$	$3.3x10^{-4}$	17.4	5.52	4.53	68	50
A10.0C d=0.45 m	7.4	$0.82x10^{-4}$	$0.68x10^{-4}$	$1.0x10^{-4}$	15.4	1.10	1.77	20	18
A15.0 no cover	65.2	$4.82x10^{-4}$	$0.87x10^{-4}$	$9.5x10^{-4}$	29.0	5.20	10.3	59	85
A15.0C d=0.85 m	11.6	$0.86x10^{-4}$	$0.68x10^{-4}$	$1.0x10^{-4}$	16.5	1.02	2.51	19	18
A20.0C d=1.20 m	15.9	$0.82x10^{-4}$	$0.68x10^{-4}$	$1.0x10^{-4}$	18.5	0.93	3.23	20	18
A30.0C d=1.50 m	21.4	$0.79x10^{-4}$	$0.05x10^{-4}$	$1.0x10^{-4}$	21.8	0.64	4.62	21	16
A10.0L1 fine part. layer	33.3	$3.7x10^{-4}$	$0.87x10^{-4}$	$22.0x10^{-4}$	20.7	5.33	7.54	422	83
A10.0L2 v. fine p.layer	57.0	$6.3x10^{-4}$	$0.87x10^{-4}$	$87.2x10^{-4}$	27.4	5.10	13.1	1785	137
A10.0 no layer	22.1	$2.45x10^{-4}$	$0.87x10^{-4}$	$3.3x10^{-4}$	17.4	5.52	4.53	68	50

TABLE IV. The symbols in the first column refer to the pile lateral dimensions and height in metres; diffusion coefficient is equal to 10^{-8} m^2/s in covers of variable thickness d. All the piles have horizontal dimensions s1=100 m, s2=90 m. The value of the reactive surface area σ per unit volume is equal to 0.5 m^{-1}. Piles A10.0L1 and A10.0L2 contain layers of thickness 0.5 m with $\sigma=2.72$ m^{-1} and $\sigma=5.44$ m^{-1}, respectively.

IX. EFFECT OF LAYERS WITH SMALL ROCK PARTICLES FORMED DUE TO EQUIPMENT TRAFFIC

In Section V we have shown that if one assumes the fractal dimension d_f=2.5 for the particle size distribution function, the rock reactivity $Rate_{surf}$ increases by a factor of 5.44 when the maximum size of particles is reduced from 50 cm to 10 cm. We use this result to analyse the large scale affect due to the meso-scale nonhomogeneity of waste rock properties. We have performed numerical simulations for piles with layers of small particles. Figs. 9.1 and 9.2 present results obtained by inserting a small-particle layer into a subcritical pile of height L=10 and σ=0.5 (pile A10.0 in Table IV). We present two scenarios. Pile A10.0L1 has a layer of thickness 0.5 m and reactivity σ=2.72. Pile A10.0L1 contains a layer of thickness 0.5 m and reactivity σ=5.44 (see Figs. 9.1 and 9.2). The results summarized in Table IV show that a single layer of fine rock particles constituting about 5% of the total waste rock mass can increase the acid generation rates by as much as 300%. When the layer absorbs water, however, the oxidation rates will be limited not by the transport of oxygen in the gas phase but by the much slower transport of oxygen in water. Therefore, in wet periods, the oxidation rates may become slower than indicated by our numerical results which do not assume the water saturation affect.

Pile A10.L1 has about a 50% faster average acid generation rate than pile A10.0 without a fine-particle layer. By raising temperature everywhere in the pile, the layers of small particles accelerate oxidation rates in the whole pile volume.

Pile A10.L2 has about a 250% faster average acid generation rate than pile A10.0 without a fine-particle layer.

The fine-particle layer in pile A10.0L2 is in a supercritical state. This is evident from plots in Fig. 9.2. Temperature distribution and acid generation rates are very nonuniform along the layer.

The small-particle regions may generate acid faster than it can be locally neutralized if the distribution of neutralizing rock is not adjusted to the method of pile construction.

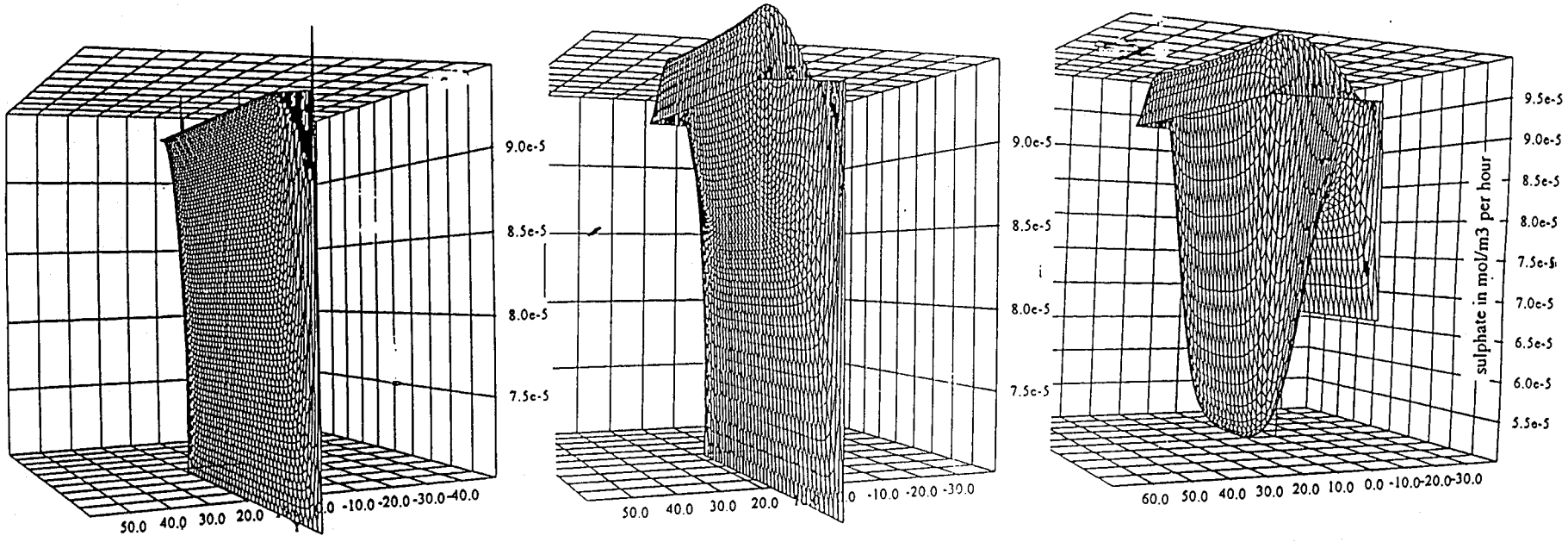

Fig. 8.1. Sulphate generation rates in piles (from left to right) A10.0C, A20.0C and A30.0C. Other results are listed in Table IV.

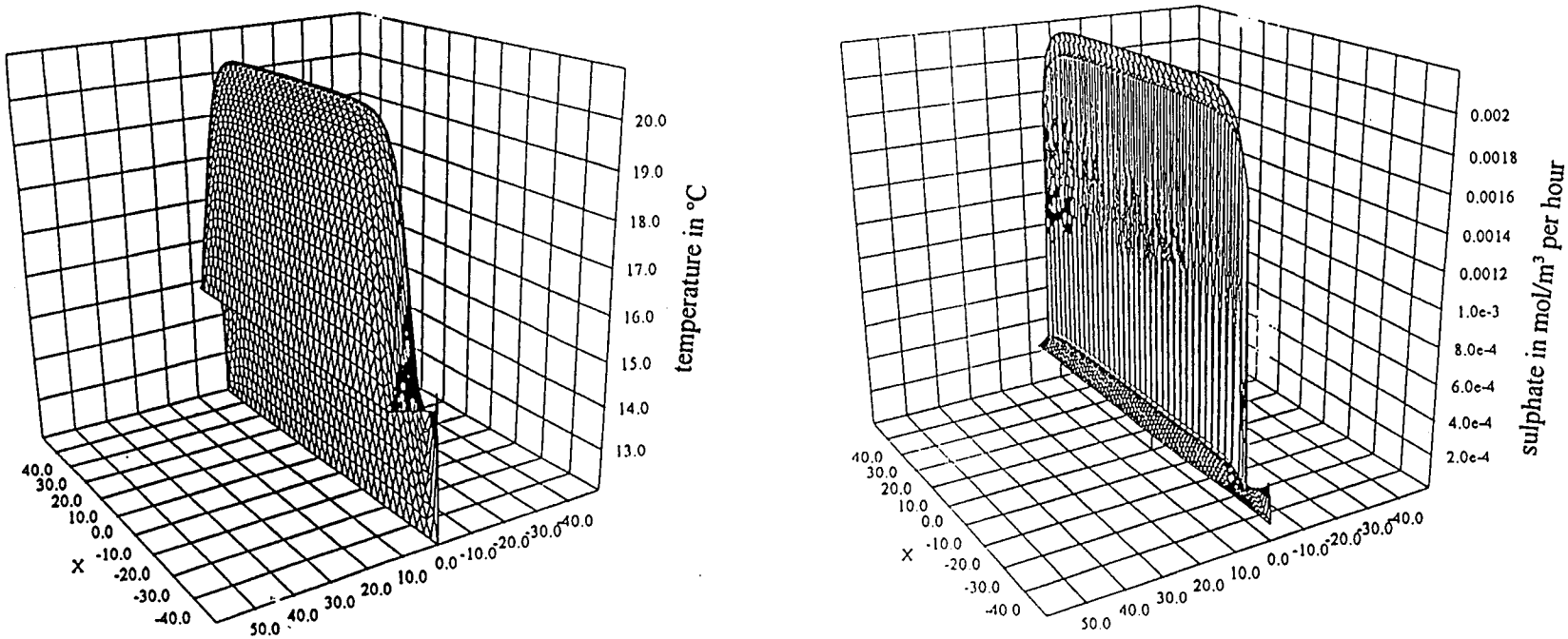

9.1. Distribution of temperature and sulphate generation rates inside pile A10.0L1 which contains a layer of fine particles with a maximum diameter five times smaller than in the rest of the pile. Layer thickness is equal to 0.5 m; rock reactivity, σ=2.72 m^{-1} in the layer is 5.44 times greater than σ=0.5 m^{-1} outside the layer. A fractal particle size distribution with d_f=2.5 is assumed.

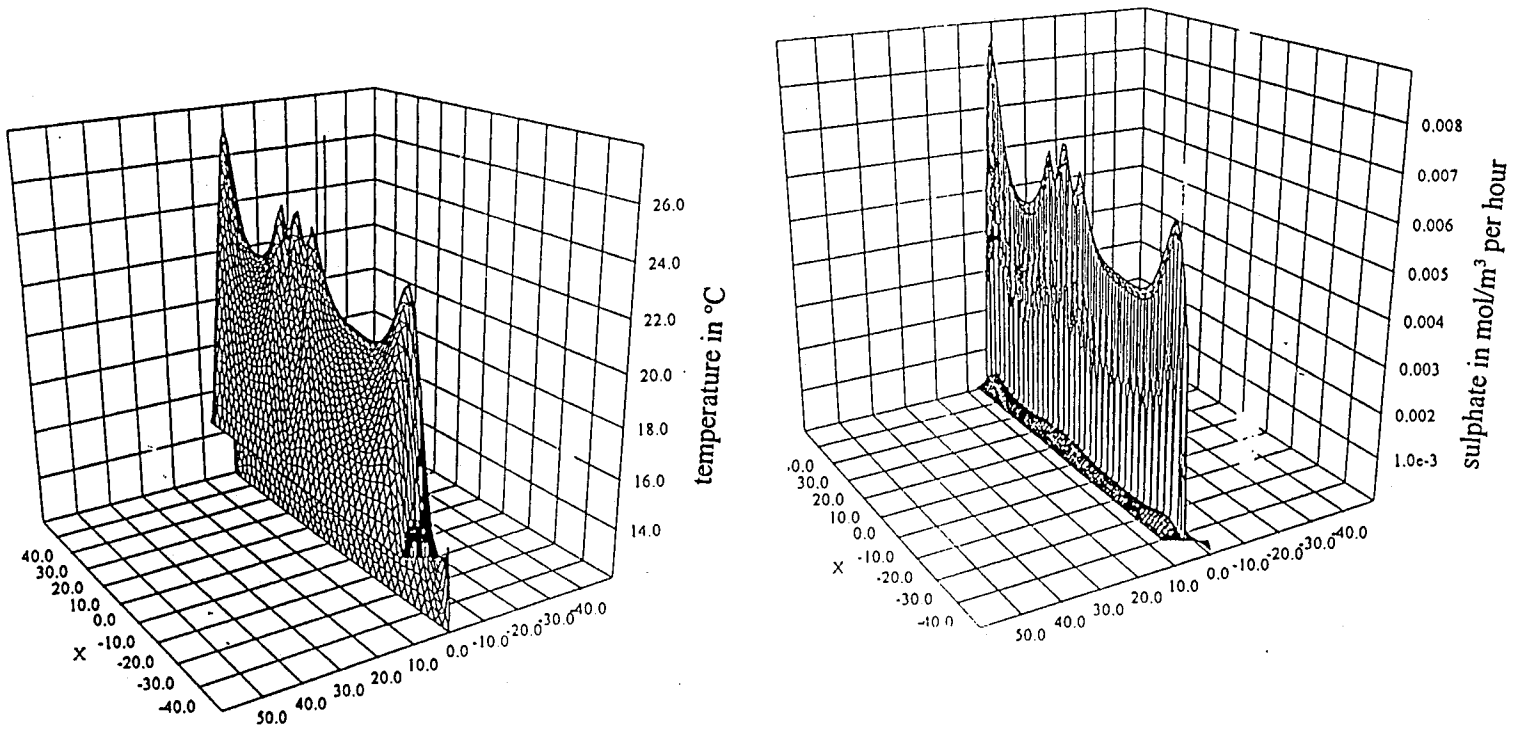

9.2. Distribution of temperature and sulphate generation rates inside pile A10.0L2 which contains very fine particles with a maximum diameter eight times smaller than in the rest of the pile. Layer thickness is equal to 0.5 m; rock reactivity σ=5.44 m^{-1} in the layer is 10.88 times greater than σ=0.5 m^{-1} outside the layer. A fractal particle size distribution with d_f=2.5 is assumed.

X. PILE HYDROLOGY

Our work on quantitative description of water flow is in progress. One of the important qualitative features of acid rock drainage is an increase of contaminants concentration with water flux as shown in Table V. In Table V , the field data from Island Copper Mine show that by increasing the water flux, concentration of contaminants often increases (i.e. no dilution is observed).

TABLE V. Trey Creek Selected Chemistry and Flow Data.

Date	Flow (l/min)	Zinc (mg/l)	Copper (mg/l)	pH	Conductivity (μmhos)
1989					
Oct 03	est 25	0.18	0.010	8.0	2100
Oct 11	est 25	0.21	0.010	8.1	1800
Oct 16	est 25	0.31	0.051	8.1	1800
Oct 17	est 25	0.31	0.020	7.5	3100
Oct 18	106	1.46	0.051	8.0	1300
Oct 23	1022	2.85	0.070	7.3	1400
Oct 30	435	2.49	0.036	7.9	1600
Nov 06	1363	4.04	0.051	7.6	1900
Nov 09	7570	3.62	0.088	6.9	1200
Nov 14	1930	8.08	0.066	7.3	2000
Nov 20	1514	5.06	0.042	7.7	1900
Nov 27	1098	4.83	0.040	7.8	1900
Dec 04	2952	4.65	0.072	7.4	1500
Dec 15	625	-	-	-	-
Dec 18	530	3.74	0.031	7.8	-
1990					
Jan 03	1172	4.02	0.052	7.7	1700
Jan 08	3634	6.20	0.120	6.8	1800
Jan 16	1665	4.60	0.062	7.4	1700
Jan 23	1968	3.50	0.068	7.2	1400
Jan 29	2460	5.40	0.072	7.4	1700
Feb 05	3596	1.80	0.094	7.6	1600
Feb 13	1741	5.20	0.070	7.7	1700
Feb 20	1022	3.60	0.040	7.8	1800
Feb 26	871	3.70	0.030	7.7	1850

SOURCE: ICM CLOSURE PLAN, 1990.

APPENDIX

Nonrandom and random fractals

Physical structures often look the same at different stages of enlargement. This property is often called scale symmetry or self-similarity. A good example of self-similar structures are branches of snow crystals which show the same structure at different magnifications. Objects which have this scale symmetry are often called fractals and are quantitatively characterized by a fractal dimension: a dimension that corresponds to the geometrical shape under study, and is often not an integer. Fractals fall naturally into two categories, nonrandom and random. Fractals in physics are random but we will first discuss nonrandom fractals in order to introduce the notion of a fractal dimension.

A1. Nonrandom fractals

(I) Sierpinski gasket

The Sierpinski gasket is a good toy model with features characteristic for aggregation processes and the self-similar properties of pores and cracks which play a significant role in acid rock drainage. A simple growth rule can be used to construct a fractal object. We closely follow the original presentation of the problem by Sierpinski (1919) (see also Stanley(1991))[1].

The Sierpinski gasket is defined algorithmically as an iterative geometric aggregation process. We use black triangular tiles, each of unit mass ($M_o=1$) and of unit edge length ($L_o=1$), to construct the series of objects illustrated in Fig. A1. At first we join vertices of three tiles to obtain a triangular object in Fig. A1b. This object has mass $M_1=3$ and edge $L_1=2$. At each subsequent step we build a new triangular object by joining the vertices of three copies of the previously obtained object. The edge length is given by the recursive formula $L_n=2L_{n-1}=2^n$ and the surface area of the whole triangular object is given by $L_n^2=2^{2n}$. At each stage (labelled by index n; n=1,2,3, ...) we analyse the density defined as

$$\rho_n(L_n)=\frac{M_n}{L_n^2}. \qquad (A1)$$

Obviously the density deceases at each iteration step. The tile in Fig. A1a has the density $\rho_o=1=3^o/2^o$. The object in Fig. A1b has the density $\rho_1=3/2^2=3^1/2^2$ (we have an object of

---

[1] Stanley, H. E. (1991). A. Bunde, & Havlin S. (ed.), Fractals and disordered systems, New York: Springer

FRACTAL DIMENSION

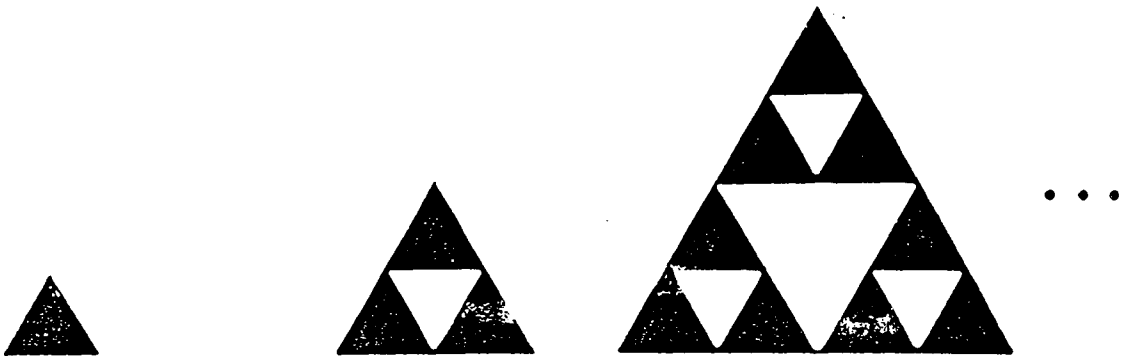

$L = 2^0$	$L = 2^1$	$L = 2^2$
$M = 3^0$	$M = 3^1$	$M = 3^2 \ldots$
$\rho = (3/4)^0$	$\rho = (3/4)^1$	$\rho = (3/4)^2$

$$\rho(L) = M(L)/L^2$$

$\rho(L)$ decreases monotonically with L, without limit, so that by iterating sufficiently we can achieve an object of as low a density as we wish

$\rho(L)$ decreases with L in a predictable fashion described by a simple power law

the surface area equal to four, with three tiles of unit mass). In stage two, three of the objects of mass $M_1=3^1$ form an object of mass $M_2=3^2$, edge $L_2=4$ and surface area $L_2^2=4^2=2^4$; in this way $\rho_2=3^2/2^4$. Object in Fig. A1c is obtained again by joining the three objects in Fig. A1b to obtain an object with mass $M_3=3^3$, surface area $L_3^2=8^2=2^6$ and the density $\rho_3=3^3/2^6$. We obviously have the rule $\rho_n=3^n/2^{2n}=(3/4)^n$ and $M_n=3^n$. We may, however, try to describe the increase of mass of the subsequent objects as the function of the edge length:

$$M_n(L_n)=AL_n^{d_f} \qquad (A2)$$

If we substitute (A2) into (A1), we find

$$\rho_n(L_n)=\frac{M_n(L_n)}{L_n^2}=AL_n^{d_f-2} \qquad (A3)$$

We can now drop the index n and write simply

$$\rho(L)=AL^{d_f-2}, \qquad (A4)$$

$$M(l)=AL^{d_f}. \qquad (A5)$$

Equation (A5) defines the fractal dimension d_f. The amplitude A is not of intrinsic interest, since it depends on the choice we made for the definitions of units for M and L. We have defined M and L so that the amplitude A is equal to one. The exponent d_f, on the other hand, depends on the rule that we follow when we iterate. Different rules give different exponents. The exponent d_f can be found by calculating the slope α ($\alpha=d_f-2$) of the plot $\rho(L)=L^{\alpha}$ in Fig. A2:

$$\alpha=slope=\frac{\log 1-\log(3/4)}{\log 1-\log 2}=\frac{\log 3}{\log 2}-2 \qquad (A6)$$

Comparing (A6) and (A5) we identify the fractal dimension of the Sierpinski gasket as

$$d_f = \frac{\log 3}{\log 2} = 1.58$$

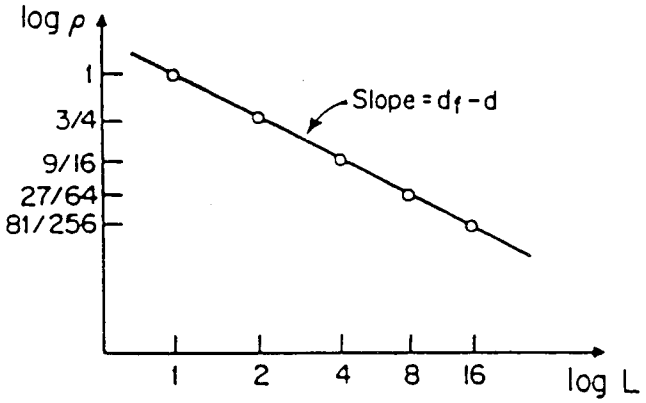

Fig. A.2. A log-log plot of ρ, the fraction of two-dimensional space covered by black tiles, as a function of L, the increasing linear size of the object.

The Sierpinski gasket has the dimension d_f smaller than the dimension of the embedding two-dimensional space. We see that the Sierpinski gasket occupies a fraction of two-dimensional space and has a dimension intermediate between that of a line (d=1) and a dimension of an area (d=2). Hence we use the term *fractal dimension* and the term *fractal* (coined by Mandelbrot) for an object with a fractal dimension.

We can construct the Sierpinski gasket in a slightly different way. We can take a single triangle of edge L and at every stage divide every black triangle in four and remove one triangle at the center. In this way the density decreases by a factor 3/4 at every iteration. The first three steps are illustrated in Fig. A3. In this way, at n-th iteration we create 3^n triangular holes, each with surface area $L^2/2^{2n}$. Without changing the external size of the object we change its density according to the rule (A4).

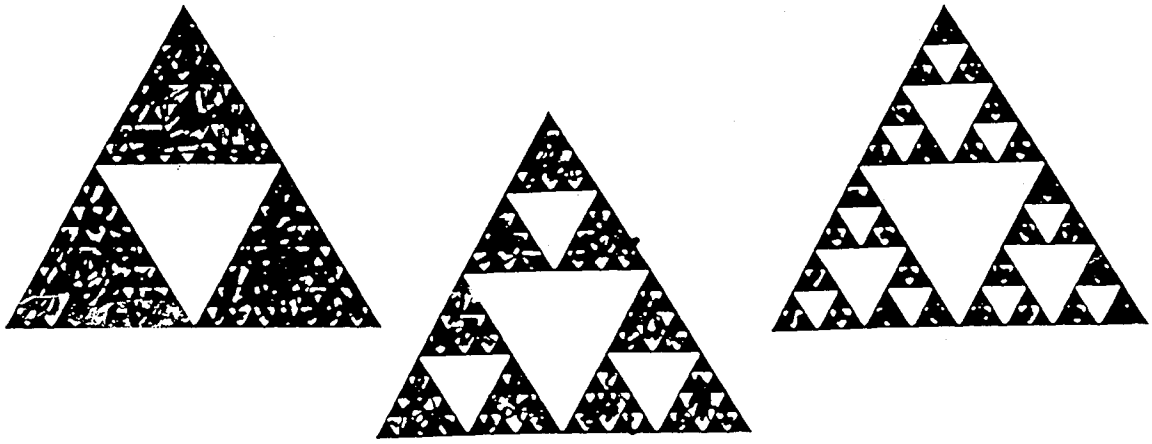

Fig. A.3. Construction of the Sierpinski gasket by dividing black triangles into four triangles and removing a triangle at the center of each divided triangle.

While in mathematics we can continue the procedure ad infinitum, in physics we hit the atomic limit after about 20 iterations. After six iterations we reach the resolution limit of the laser printer used to produce this page. After eight iterations we reach the resolution limit of the human eye. In practice we often detect fractal properies of physical objects by analyzing an object at different magnification scales or by increasing the resolution of our observation device. Fig. A3a can can be viewed as a picture seen by an observer for whom it is impossible to see objects on scales smaller than L. Increasing resolution twice, an observer can see the same fractal object as the object in Fig A3b, with features on scale L/2. Increasing the resolution twice again, an observer would see features on scale L/4. Thus by improving the resolution, an observer can analyze the density for the black part of the fractal object and reconstruct the plot A.2 with the log of magnification scale instead of logL along the horizontal axis.

Looking at a mathematical fractal we could double the magnification infinitely many times and at every stage we would see the same object. For this reason fractal structures are said to be scale-invariant or self-similar. We use the self-similarity property to analyze the fractal dimension of fragmented rock. For physical fractal objects the self-similarity ceases to exist at sufficiently large magnifications. The fractal nature of physical objects can be often observed in simple experiments over 2-4 orders of magnitude. When the slope

of the logρ vs. logL plot changes at a certain point we say that a physical object is *multifractal.*

(ii) Menger sponge

The Menger sponge is a fractal object embedded in three dimensions. The Menger sponge has cubic voids on all scales smaller than the size of the initial cube used for the iterative construction. It has been used as a simple fractal model for porous media. The iterative algorithm is illustrated in Fig. A.4. A solid cube is of unit dimension and has square passagees with dimensions $r_1=1/3$ cut through the centers of the six sides. The six cubes in the cubes with dimensions $r_1=1/3$ are removed as well as the central cube. Twenty out of 27 cubes with dimensions $r_1=1/3$ are retained so that $N_1=20$. At second order $r_2=1/9$ and 400 out of 729 cubes are retained so that $N_2=400$. The value of fractal dimension is $d_f=2.7268$. The menger sponge has been used as a model for flow in porous media with a fractal distribution of porosity. We do not consider however the Menger sponge, and other similar geometric models with large porosity values, to be a good representation of physical situation in porous media. Many rocks show a nonzero permeability at porosity values below 10%, much smaller than mathematical models using geometric fractals. (See also discussion in Chapter II).

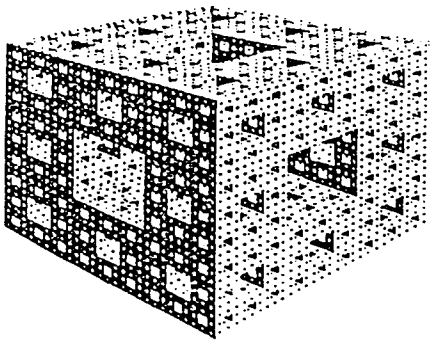

Fig. A4. Menger sponge.

A2. Random fractals

Physical objects are random fractals. This means that parts of a fractal are randomly arranged. One could easily construct a random fractal by randomly rotating black tiles in the Sierpinski gasket and slightly deforming individual tiles. There is experimental evidence indicating that porous rock has a fractal porous structure. Fig. A.6 shows the structure of sandstone observed by using an electron scanning microscope. The difficulty of ordering different magnifications is an indication of self-similarity of pore structure. For a given magnification scale the surface area of the observed features can be measured by using grids of increasing resolution. At each resolution scale, the area S_n of the analyzed features can be measured in units of the elementary squares of a grid. We count all squares which contain the elements of the analyzed structure. Next we choose many different local origins for our window boxes to obtain good statistics. The results of the measurments at different scales can then be expressed in units L_{min}^2 of the area of the squares in the finest grid. The results can be plotted as logM vs. log (L_n/L_{min}) and the fractal dimension is obtained as the slope d_f (see formula (A3).

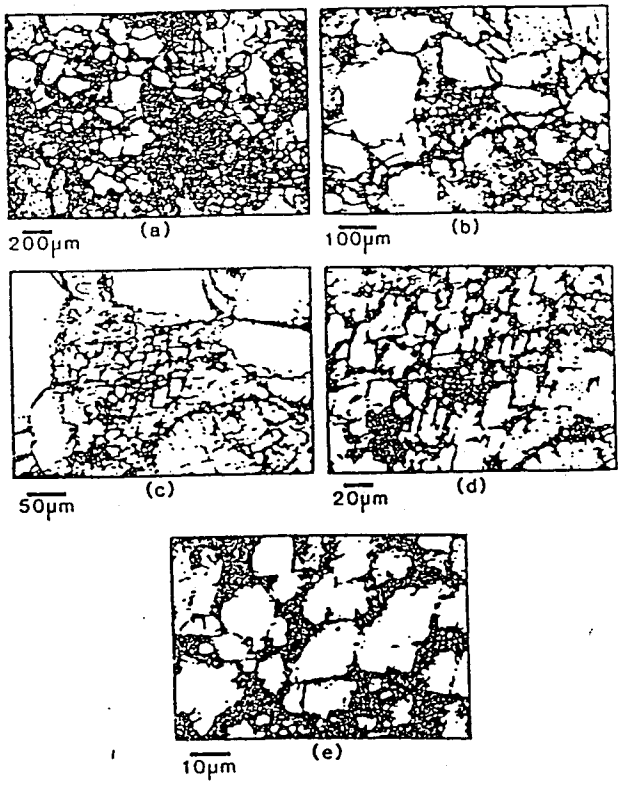

Fig. A6. Fractal structure of sandstone.

It is worth noting that the fractal dimension of an ensemble of fractal objects is not necessarily a fractal object on all scales. Physical objects may show a crossover from the fractal character at small length scales to a homogeneous behaviour at large length scales. This property is illustrated in Fig. A7 by a hexagonal lattice of Sierpinski gasket cells of size ξ. On a length scale smaller than ξ, we see a fractal structure. On length scales larger than ξ, we see a homogeneous system which is translationally invariant for translations by integer multiplicities of ξ.

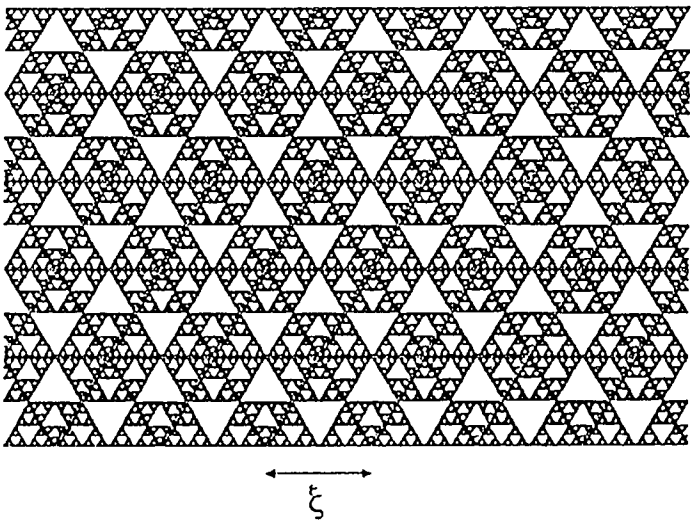

Fig. A7. Lattice of Sierpinski gaskets.

Now imagine a situtuation in which we spoil the perfect order of the lattice in Fig. A7. Lets us randomly rotate and translate individual cells, thus arranging them in a random manner. Such a system becomes invariant (in a statistical sense) with respect to translations by an arbitrary distance, i.e. the system looks the same from any reference point. The contact with the properties of a waste rock pile can be made if we interpret each of the hexagonal cells as an object analogous to a porous rock particle of size ξ - we can call each cell a "Sierpinski particle". To make our construction more realistic we break the individual cells into fragments which have a size distribution with a fractal dimension d_r different than the fractal dimension d_f of pores in individual "Sierpinski particles". Such an ensemble has multifractal features. On length scales greater than the maximum size of particles, the

system is homogeneous. On scales smaller than the size of the largest particles but greater then the pore size, the system has the fractal dimension d_r. Individual particles have the fractal dimension d_f. The process of rock fragmentation is often described in terms of formation and growth of cracks. Because there is experimental evidence that pores and preexisting cracks (cracks which exist before blasting) can be characterized by the fractal dimension, one might expect a relation between the fractal dimensions of pores and cracks and a fractal dimension describing the particle size distribution. To our knowledge no analysis of this problem has been performed.

For a more rigorous presentation based on the topological concepts and Haussdorf dimension we refer the reader to Mandelbrot:

Mandelbrot (1983). The fractal geometry of nature, Freeman, San Francisco (1983)

Mandelbrot, & B.B. (1989). *An Overview of the Language of Fractals*, in Avnir, & D. The Fractal Approach to Heterogeneous Chemistry, . Wiley.